The Journal of Chemical Physics

Multiscale relaxation dynamics and diffusion of myelin basic protein in solution studied by quasielastic neutron scattering

Cite as: J. Chem. Phys. **156**, 025102 (2022); https://doi.org/10.1063/5.0077100
Submitted: 30 October 2021 • Accepted: 19 December 2021 • Accepted Manuscript Online: 22 December 2021 • Published Online: 11 January 2022

Abir N. Hassani, Luman Haris, Markus Appel, et al.

The Journal of Chemical Physics ARTICLE scitation.org/journal/jcp

Multiscale relaxation dynamics and diffusion of myelin basic protein in solution studied by quasielastic neutron scattering

Cite as: J. Chem. Phys. 156, 025102 (2022); doi: 10.1063/5.0077100
Submitted: 30 October 2021 • Accepted: 19 December 2021 •
Published Online: 11 January 2022

Abir N. Hassani,[1,2,3] Luman Haris,[3,4] Markus Appel,[5] Tilo Seydel,[5] Andreas M. Stadler,[3,4,a)] and Gerald R. Kneller[1,2,b)]

AFFILIATIONS

[1] Centre de Biophysique Moléculaire, CNRS and Université d'Orléans, Rue Charles Sadron, 45071 Orléans, France
[2] Synchrotron Soleil, L'Orme de Merisiers, 91192 Gif-sur-Yvette, France
[3] Jülich Centre for Neutron Science (JCNS-1) and Institute of Biological Information Processing (IBI-8), Forschungszentrum Jülich GmbH, 52425 Jülich, Germany
[4] Institute of Physical Chemistry, RWTH Aachen University, Landoltweg 2, 52056 Aachen, Germany
[5] Institut Laue Langevin, 71 Avenue des Martyrs, 38042 Grenoble Cedex 9, France

[a)] **E-mail:** a.stadler@fz-juelich.de
[b)] **Author to whom correspondence should be addressed:** gerald.kneller@cnrs.fr

ABSTRACT

We report an analysis of high-resolution quasielastic neutron scattering spectra from Myelin Basic Protein (MBP) in solution, comparing the spectra at three different temperatures (283, 303, and 323 K) for a pure D_2O buffer and a mixture of D_2O buffer with 30% of deuterated trifluoroethanol (TFE). Accompanying experiments with dynamic light scattering and Circular Dichroism (CD) spectroscopy have been performed to obtain, respectively, the global diffusion constant and the secondary structure content of the molecule for both buffers as a function of temperature. Modeling the decay of the neutron intermediate scattering function by the Mittag-Leffler relaxation function, $\phi(t) = E_\alpha(-(t/\tau)^\alpha)$ $(0 < \alpha < 1)$, we find that trifluoroethanol slows down the relaxation dynamics of the protein at 283 K and leads to a broader relaxation rate spectrum. This effect vanishes with increasing temperature, and at 323 K, its relaxation dynamics is identical in both solvents. These results are coherent with the data from dynamic light scattering, which show that the hydrodynamic radius of MBP in TFE-enriched solutions does not depend on temperature and is only slightly smaller compared to the pure D_2O buffer, except for 283 K, where it is much reduced. In accordance with these observations, the CD spectra reveal that TFE induces essentially a partial transition from β-strands to α-helices, but only a weak increase in the total secondary structure content, leaving about 50% of the protein unfolded. The results show that MBP is for all temperatures and in both buffers an intrinsically disordered protein and that TFE essentially induces a reduction in its hydrodynamic radius and its relaxation dynamics at low temperatures.

I. INTRODUCTION

Since the 1990s, the literature has seen a considerable increase in studies targeting the so-called intrinsically disordered proteins (IDPs), which have a well-defined function but not a well-defined structure.[1–4] The discovery of IDPs marked a change of the long-standing paradigm in structural biology that a protein structure is a prerequisite for the protein function. A protein is usually considered intrinsically disordered if it contains at least one region of 40 consecutive amino acids that do not correspond to any particular secondary structure (α-helix or β-strand). One of the prominent members of the family of IDPs is Myelin Basic Protein (MBP), which is the basic constituent of the myelin sheath of nerves and the second most abundant protein in the central nervous system. The protein plays an important role in understanding diseases of the human nervous system, such as multiple sclerosis. In its predominant form, MBP contains 170 residues and has a molecular weight of 18.5 kDa. In aqueous solution, the protein is intrinsically disordered, and the

present study focusses on the effect of trifluoroethanol (TFE)–water mixtures on its global and internal dynamics. TFE is used since many years as an agent, which is known to induce the formation of α-helices in IDPs, but its action is still not completely understood. The formation of secondary structure elements does, for instance, not necessarily lead to a well-defined global native structure as for globular proteins.[5] The aim of the present quasielastic neutron scattering (QENS) study is to shed some light on the action of TFE on the global folding and the dynamics of MBP. Thermal neutron scattering is a unique technique to study the structural dynamics of condensed matter at the atomic scale, including soft matter and biological molecules. The energy of thermal neutrons matches by definition the thermal energies of atoms in condensed matter systems, and its wavelength is compatible with typical interatomic distances. High-resolution quasielastic neutron scattering (QENS), with typical resolutions in the μeV range, corresponding to a few nanoseconds, is, in particular, suitable to study the slow internal relaxation dynamics of complex macromolecular systems.[6–8] We mention here that QENS is complementary to neutron spin-echo spectroscopy, which probes macromolecular conformational dynamics on much longer time scales of up to several hundred nanoseconds and which has also been applied previously to study the dynamics of MBP.[9,10]

The internal dynamics of proteins and complex molecular systems, in general, is characterized by a strongly non-exponential relaxation of the relevant time correlation functions, which exhibit an asymptotic power law decay. The power law decay reflects self-similarity, i.e., forms invariance of the correlation functions under a change of the time scale, which is also typical for glasses.[11–19] The typical properties of internal protein dynamics described above must be taken into account in the model for QENS from MBP, and the challenge is that the dynamics of very slow relaxation modes overlaps with elastic scattering[20] and also with the diffusion of whole molecules, which must be taken into account since MBP is studied in solution. For this purpose, we extend a model for internal protein dynamics, which has been recently used to analyze QENS data from protein powder samples of human acetylcholinesterase.[21,22]

This paper is organized as follows: Sec. II describes the experimental details and is followed by a presentation of the model for the intermediate scattering function, a discussion of the results, and a conclusion, which are, respectively, presented in Secs. III–V.

II. EXPERIMENTS

A. QENS spectra

1. Sample preparation

Bovine Myelin Basic Protein (MBP) and all used chemicals were bought from Sigma-Aldrich (St. Louis, MO, USA). MBP powder was dissolved in D_2O (99.9 at. % D) and incubated for one day to allow for exchange of liable protons. The MBP solution was then again freeze dried. The QENS experiments have been performed for D_2O-exchanged MBP in solution, using for the latter a D_2O buffer (20 mM Na_2HPO_4/NaH_2PO_4, pH 4.8) and a corresponding D_2O buffer with 30 vol. % per volume of deuterated 2,2,2-trifluoroethanol-d3 (TFE). The protein concentration was 55 mg/ml. The protein concentration was determined by optical absorption at 280 nm wavelength with an absorbance of $E_{1\%} = 5.89$.[23]

2. Instrument

All QENS spectra have been collected on the IN16B spectrometer operated by the Institut Laue-Langevin in Grenoble. IN16B is a neutron backscattering spectrometer with a new "BATS mode" (Backscattering And Time of flight Spectrometer) that considerably extends the accessible energy transfer range.[24,25] The data have been collected for three different temperatures, 283, 303, and 323 K, with an energy resolution of 3.5 μeV, an energy transfer range of ± 150 μeV, and a momentum transfer range of $0.8\ \text{Å}^{-1} < q < 1.8\ \text{Å}^{-1}$ in units of $\hbar$. All samples and buffers were measured in annular aluminum sample holders with a gap thicknesses of 0.3 mm. The QENS data of the samples were normalized by the vanadium reference, and the data reduction was performed with the MANTID software.[26]

B. Accompanying experiments

Accompanying experiments with dynamic light scattering (DLS) and Synchrotron Radiation Circular Dichroism (SRCD) spectroscopy have been performed to estimate, respectively, the global diffusion coefficient of MBP and its secondary structure content as a function of temperature and buffer. The details are described in the supplementary material, and we mention here only the respective protein concentrations that were used in the experiments since they are important for the discussion of the results.

Concerning the DLS experiments, we used a protein concentration of 4 mg/ml for the pure D_2O buffer and 7 mg/ml for the D_2O buffer with 30% TFE. We found that MBP coagulates T = 323 K in the pure D_2O buffer, which manifests itself in a drastic decrease in the measured diffusion constant. Therefore, we replaced the latter for subsequent data analysis by an estimate through linear extrapolation from smaller temperatures (see the supplementary material). The SRCD spectra were recorded with 44 mg/ml for the pure D_2O buffer and with 20 mg/ml for the D_2O buffer with 30% TFE.

III. THEORY AND DATA ANALYSIS

A. Scattering functions

Thermal neutron scattering probes the differential scattering cross section of the sample under consideration,

$$\frac{d^2\sigma}{d\Omega d\omega} = \frac{k}{k_0}\mathcal{S}(\mathbf{q},\omega), \tag{1}$$

where k_0 and k are the momenta of the incident and scattered neutrons, respectively, in units of $\hbar$ and $\mathcal{S}(\mathbf{q},\omega)$ is the dynamic structure factor. The latter depends on the kinematical variables $\mathbf{q}$ and ω, which are, respectively, the momentum and energy transfer from the neutron to the sample. It can be written as the time Fourier transform of the intermediate scattering function,

$$\mathcal{S}(\mathbf{q},\omega) = \frac{1}{2\pi}\int_{-\infty}^{+\infty} dt e^{-i\omega t}\mathcal{F}(\mathbf{q},t), \tag{2}$$

which splits into a coherent and an incoherent part,

$$\mathcal{F}(\mathbf{q},t) = \mathcal{F}_{\text{coh}}(\mathbf{q},t) + \mathcal{F}_{\text{inc}}(\mathbf{q},t), \tag{3}$$

containing, respectively, the information about the collective and average single-atom dynamics of the scattering system,

$$\mathcal{F}_{\rm coh}(\mathbf{q},t) = \frac{1}{N}\sum_{i,j} b^*_{i,\rm coh} b_{j,\rm coh} \left\langle e^{-i\mathbf{q}\cdot\hat{\mathbf{R}}_i(0)} e^{i\mathbf{q}\cdot\hat{\mathbf{R}}_j(t)} \right\rangle, \tag{4}$$

$$\mathcal{F}_{\rm inc}(\mathbf{q},t) = \frac{1}{N}\sum_{i} b^2_{i,\rm inc} \left\langle e^{-i\mathbf{q}\cdot\hat{\mathbf{R}}_i(0)} e^{i\mathbf{q}\cdot\hat{\mathbf{R}}_i(t)} \right\rangle. \tag{5}$$

Here, $\hat{\mathbf{R}}_i(t)$ denotes the position operator of atom i, $\langle\cdots\rangle$ denotes a quantum ensemble average, and $b_{i,\rm coh}$ and $b_{i,\rm inc}$ are the coherent and incoherent scattering lengths of atom i, respectively.[7,27] Being the quantum time correlation function, the intermediate scattering verifies the symmetry relation

$$\mathcal{F}(\mathbf{q},t) = \mathcal{F}(-\mathbf{q}, -t + i\beta\hbar), \tag{6}$$

which translates into the detailed balance relation

$$\mathcal{S}(\mathbf{q},\omega) = \mathcal{S}(-\mathbf{q},-\omega) e^{\beta\hbar\omega/2} \tag{7}$$

for the dynamic structure factor.

Protein solutions are isotropic systems, and the total observed dynamic structure factor may be expressed as an isotropic angular average over all directions of $\mathbf{q}$,

$$\mathcal{S}_{\rm tot}(q,t) = \overline{\mathcal{S}_{\rm tot}(\mathbf{q},t)} = \frac{1}{4\pi}\iint \sin(\theta) d\theta d\phi\, \mathcal{S}_{\rm tot}(q\mathbf{n}(\theta,\phi),t). \tag{8}$$

Here, $\mathbf{n}_q = (\sin\theta\cos\phi,\ \sin\theta\sin\phi, \cos\theta)$ is the unit vector pointing into the direction of $\mathbf{q}$ and $q \equiv |\mathbf{q}|$. The QENS spectra of MBP were then extracted according to

$$\mathcal{S}_{\rm protein}(q,\omega) \approx \mathcal{S}_{\rm tot}(q,\omega) - (1-\phi)\mathcal{S}_{\rm buffer}(q,\omega), \tag{9}$$

using that the partial specific volume of the protein is $\overline{v} = 0.73$ ml/g. For a concentration of $c = 55$ mg/ml, this leads to a volume fraction for the protein of $\phi = c\overline{v} = 0.040\,15$ (see Ref. 28). Since the incoherent neutron scattering from hydrogen dominates by far the coherent and incoherent scattering from all other atoms, the dynamic structure factor for MBP may be approximated by

$$\mathcal{S}_{\rm protein}(q,\omega) \approx b^2_{H,\rm inc} S_{H,\rm protein}(q,\omega), \tag{10}$$

and we abbreviate in the following $S(q,\omega) \equiv S_{H,\rm protein}(q,\omega)$, i.e.,

$$S(q,\omega) \equiv \frac{1}{2\pi}\int_{-\infty}^{+\infty} dt e^{-i\omega t} F(\mathbf{q},t), \tag{11}$$

$$F(q,t) = \frac{1}{N}\sum_{i\in \rm protein H} \overline{\left\langle e^{-i\mathbf{q}\cdot\widehat{\mathbf{R}}_i(0)} e^{i\mathbf{q}\cdot\widehat{\mathbf{R}}_i(t)} \right\rangle}. \tag{12}$$

The above definition shows that

$$\int_{-\infty}^{+\infty} d\omega\, S(q,\omega) = 1 = F(q,0), \tag{13}$$

and this normalization will be used in the following.

B. Symmetrization of the QENS spectra

For the further data analysis, we will be using the symmetrized dynamic structure factor

$$S^{(+)}(q,\omega) = \frac{e^{-\beta\hbar\omega/2} S(q,\omega)}{\int_{-\infty}^{+\infty} d\omega\, e^{-\beta\hbar\omega/2} S(q,\omega)}, \tag{14}$$

which is an even function in ω and which is normalized such that

$$\int_{-\infty}^{+\infty} d\omega\, S^{(+)}(q,\omega) = F^{(+)}(q,0) = 1. \tag{15}$$

The corresponding intermediate scattering function is a symmetric function in time,

$$F^{(+)}(q,t) = \frac{F(q,t+i\beta\hbar/2)}{F(q,i\beta\hbar/2)}, \tag{16}$$

and we note in this context that $S^{(+)}(q,\omega) \approx S^{(cl)}(q,\omega)$ and $F^{(+)}(q,t) \approx F^{(cl)}(q,t)$ correspond to Schofield's semiclassical approximation,[29] where the superscript "(cl)" indicates the corresponding classical scattering function. With this reasoning essentially, classical models can be used for the interpretation of QENS spectra.

C. Resolution deconvolution

The experimental dynamic structure factor, denoted by an index "m," can be written as the convolution of the "ideal" dynamic structure factor and the instrumental resolution plus a noise,

$$S^{(+)}_m(q,\omega) = \int_{-\infty}^{+\infty} d\omega' S^{(+)}(q,\omega-\omega')\tilde{R}(q,\omega') + \tilde{N}(q,\omega), \tag{17}$$

where $\tilde{N}(q,\omega)$ and $\tilde{R}(q,\omega)$ represent the noise and the instrumental resolution, respectively, and are supposed to be symmetric in ω. In the context of this paper, $\tilde{R}(q,\omega) = S^{(+)}_{\rm vanadium}(q,\omega)$ is the symmetrized dynamic structure factor of a vanadium sample with identical dimensions to the sample of interest, and the noise is essentially unknown. Here, one uses the fact that vanadium can be considered as an ideal isotropic and elastic scatterer. In the time domain, Eq. (17) becomes

$$F^{(+)}_m(q,t) = F^{(+)}(q,t)R(q,t) + N(q,t), \tag{18}$$

noting that the convolution term in ω becomes a normal product. The "ideal" resolution corrected intermediate scattering function is therefore obtained through

$$F^{(+)}(q,t) = \frac{F^{(+)}(q,t)}{R(q,t)} - \frac{N(q,t)}{R(q,t)}. \tag{19}$$

The above equation shows that the limit of the instrumental deconvolution by Fourier transform is set by the term $N(q,t)/R(q,t)$, which becomes dominant for small values of the resolution window, $R(q,t)$. In practice, the threshold for $R(q,t)$ is attained for

$$t_{\rm max} \approx \frac{h}{2\Delta\omega}, \tag{20}$$

where h is Planck's constant and $\Delta\omega$ is the instrumental energy resolution. For the IN16B spectrometer, on which the QENS data analyzed in this paper have been recorded, we have $\Delta\omega = 3.5$ μeV, corresponding to $t_{\rm max} \approx 600$ ps. Figure 1 illustrates the spectral

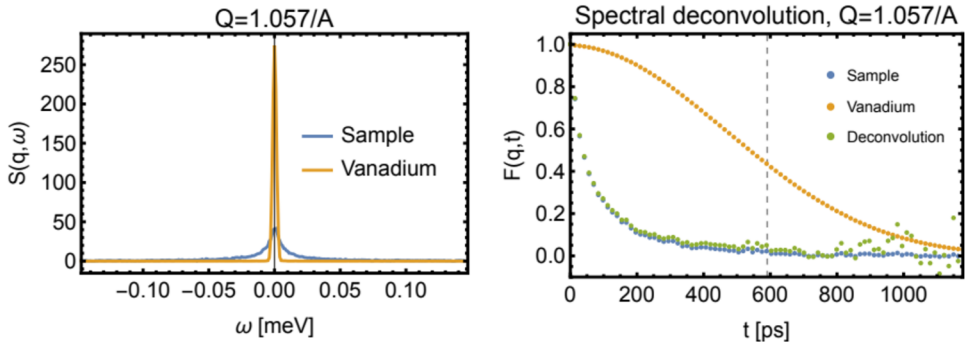

FIG. 1. Left panel: Symmetrized and normalized dynamic structure factor, $S_m^{(+)}(q,\omega)$, of MBP in D_2O buffer at $q = 1.06$ Å^{-1} and T = 283 K (blue line) with the corresponding resolution function $\tilde{R}(q,\omega)$ (dark yellow line) obtained from a vanadium run. Right panel: Corresponding intermediate scattering function, $F_m^{(+)}(q,t)$, in the time domain (dark yellow dots) and resulting deconvoluted intermediate scattering function $F^{(+)}(q,t)$ (green dots). The vertical dashed line indicates the accessible time domain corresponding to the resolution of the instrument [Eq. (20)].

deconvolution for the QENS spectrum of MBP in D_2O buffer for T = 283 K at $q = 1.057/\text{Å}$. In the left panel, we show the symmetrized and normalized dynamic structure factor $S_m^{(+)}(q,\omega)$ (blue line) together with the corresponding spectrum of vanadium, $\tilde{R}(q,\omega)$, which defines the instrumental resolution (dark yellow line). Here, individual data points cannot be resolved for the full accessible ω-range. The right panel displays the corresponding intermediate scattering functions, $F_m^{(+)}(q,t)$ (blue dots) and $R(q,t)$ (dark yellow dots), which have been obtained by discrete (Fast) Fourier transform from equidistantly sampled arrays representing $S_m^{(+)}(q,\omega)$ and $\tilde{R}(q,\omega)$. The resolution-deconvoluted intermediate scattering function, $F^{(+)}(q,t)$, is given by the green dots, and the dashed vertical line indicates the threshold of $t_{\max} \approx 600$ ps corresponding to the instrumental resolution. All displayed data points fulfilling $t \le t_{\max}$ have been used for the fit of the model to be described in the following.

D. QENS model

1. Generic form of the intermediate scattering function

The data analysis of the QENS spectra from intrinsically disordered proteins presents the difficulty that the center-of-mass motion and the motions relative to the center of mass are entangled. Here, we use the simplest approximation of the intermediate scattering function that consists in neglecting this entanglement in the functional form,

$$F^{(+)}(q,t) \approx e^{-Dq^2|t|} F_{\text{int}}^{(+)}(q,t), \tag{21}$$

and considering D to be an *apparent* translational diffusion coefficient that also contains contributions from motions relative to the center of mass. The intermediate scattering function for the internal dynamics of MBP has the generic form

$$F_{\text{int}}^{(+)}(q,t) = EISF(q) + (1 - EISF(q))\phi^{(+)}(q,t), \tag{22}$$

where the symbol $EISF(q)$ stands for the elastic incoherent structure factor,

$$EISF(q) = \frac{1}{N}\sum_{i\in H}\overline{\left|\left\langle e^{i\mathbf{q}\cdot\hat{\mathbf{R}}_i}\right\rangle\right|^2}, \tag{23}$$

and $\phi^{(+)}(q,t)$ describes the relaxation of $F^{(+)}(\mathbf{q},t)$ toward this plateau value. Introducing the fluctuation of the Fourier transformed density of atom i,

$$\delta\rho_i(\mathbf{q},t) = e^{i\mathbf{q}\cdot\hat{\mathbf{R}}_i(t)} - \left\langle e^{i\mathbf{q}\cdot\hat{\mathbf{R}}_i}\right\rangle, \tag{24}$$

the relaxation function $\phi(q,t)$ can be explicitly expressed as a normalized quantum time correlation function,

$$\phi(q,t) = \overline{\left(\frac{\sum_{i\in H}\langle\delta\rho_i^\dagger(\mathbf{q},0)\delta\rho_i(\mathbf{q},t)\rangle}{\sum_{i\in H}\langle\delta\rho_i^\dagger(\mathbf{q},0)\delta\rho_i(\mathbf{q},0)\rangle}\right)}, \tag{25}$$

and its Fourier transform

$$\tilde{\phi}(q,\omega) = \frac{1}{2\pi}\int_{-\infty}^{+\infty} dt\, e^{-i\omega t}\phi(q,t) \tag{26}$$

leads to

$$S_{\text{int}}(q,\omega) = EISF(q)\delta(\omega) + (1 - EISF(q))\tilde{\phi}(q,\omega), \tag{27}$$

which shows explicitly that the EISF determines the elastic component of the QENS spectrum for the internal protein dynamics.

2. Multiscale relaxation

The internal dynamics in MBP is described by a Mittag-Leffler (ML) relaxation function,[18,19]

$$\phi_{\text{ML}}^{(+)}(t) = E_\alpha\left(-(|t|/\tau_R)^\alpha\right), \qquad 0 < \alpha < 1, \tag{28}$$

where the q-dependence is omitted for better readability. Here, $E_\alpha(\cdot)$ is the Mittag-Leffler (ML) function,[30] which is defined by the Taylor series,

$$E_\alpha(z) = \sum_{n=0}^{\infty}\frac{z^n}{\Gamma(1+\alpha n)} \quad (\alpha > 0), \tag{29}$$

for all arguments in the complex plane. For $0 < \alpha \le 1$, the ML relaxation function (28) decays monotonously, with an asymptotically power law form,

$$\phi_{\mathrm{ML}}(t) \overset{t\gg\tau_R}{\sim} \frac{(t/\tau_R)^{-\alpha}}{\Gamma(1-\alpha)}, \tag{30}$$

and exponential relaxation is retrieved for $\alpha = 1$,

$$\lim_{\alpha\to 1}\phi_{ML}(t) = \exp(-|t|/\tau), \tag{31}$$

where the power-law long time tail vanishes.

Since the Laplace transform of the ML relaxation function has a simple analytical form,[30]

$$\hat{\phi}_{\mathrm{ML}}(s) = \frac{1}{s(1+(s\tau_R)^{-\alpha})}, \tag{32}$$

its Fourier and relaxation rate spectra can be easily obtained through

$$\phi^{(+)}(\omega) = \lim_{\epsilon\to 0}\frac{1}{\pi}\Re\left\{\hat{\phi}^{(+)}(i\omega+\epsilon)\right\}, \tag{33}$$

which leads to a "generalized Lorentzian,"[31]

$$\tilde{\phi}_{\mathrm{ML}}(\omega) = \frac{1}{\pi}\frac{\sin\left(\frac{\pi\alpha}{2}\right)}{|\omega|\left((|\omega|\tau_R)^{-\alpha}+(|\omega|\tau_R)^{\alpha}+2\cos\left(\frac{\pi\alpha}{2}\right)\right)}. \tag{34}$$

Here, $\int_{-\infty}^{+\infty} d\omega\, \tilde{\phi}_{\mathrm{ML}}(\omega) = 1$, and the standard Lorentzian is retrieved for $\alpha \to 1$. It should be noted that $\tilde{\phi}_{\mathrm{ML}}(\omega) \sim |\omega|^{\alpha-1}$ for $\omega \to 0$ and becomes thus singular for $0 < \alpha < 1$.

The Laplace transform (32) of the ML relaxation function can also be used to obtain an analytical form of its relaxation rate spectrum. For an arbitrary monotonously decaying relaxation function, $\phi(t)$, the latter is defined through the relation

$$\phi(t) = \int_0^\infty d\lambda\, p(\lambda)\exp(-\lambda|t|), \tag{35}$$

where $p(\lambda) \geq 0$ and $\int_0^\infty d\lambda\, p(\lambda) = 1$. Using that

$$p(\lambda) = \lim_{\epsilon\to 0}\frac{1}{\pi}\Im\left\{\hat{\phi}^{(+)}(-\lambda - i\epsilon)\right\}, \tag{36}$$

one finds for the ML relaxation function[31]

$$p_{\mathrm{ML}}(\lambda) = \frac{\sin(\pi\alpha)}{\pi\lambda((\lambda\tau_R)^{-\alpha}+(\lambda\tau_R)^{\alpha}+2\cos(\pi\alpha))}. \tag{37}$$

The slow power law decay (28) of $\phi_{\mathrm{ML}}(t)$ leads here to a power law form of the relaxation rate spectrum for small arguments, $p_{\mathrm{ML}}(\lambda) \overset{\lambda\to 0}{\sim} \lambda^{\alpha-1}$.

3. Total dynamic structure factor

Using the general form (21) of the total intermediate scattering function, we write the symmetrized version in the form

$$F^{(+)}(t) = e^{-\epsilon|t|}(EISF + (1-EISF)\phi_{\mathrm{ML}}(|t|)), \tag{38}$$

omitting again the q-dependence in the formulas and defining

$$\epsilon := Dq^2. \tag{39}$$

The dynamic structure factor can then be expressed in terms of the Laplace transformed intermediate scattering function,

$$S^{(+)}(\omega) = \frac{1}{\pi}\Re\left\{\hat{F}^{(+)}(i\omega+\epsilon)\right\}, \tag{40}$$

which leads to

$$S^{(+)}(\omega) = EISF\,\frac{1}{\pi}\frac{\epsilon}{\omega^2+\epsilon^2} + (1-EISF)\,\tilde{\phi}^{(\epsilon)}_{\mathrm{ML}}(|\omega|), \tag{41}$$

where $\tilde{\phi}^{(\epsilon)}_{\mathrm{ML}}(\omega)$ is the Fourier transform of the diffusion-damped ML relaxation function,[32]

$$\tilde{\phi}^{(\epsilon)}_{\mathrm{ML}}(\omega) = \frac{\epsilon\left(\omega^2+\epsilon^2\right)^{\alpha/2} + \omega\,\sin(\alpha\arg(\epsilon+i|\omega|)) + \epsilon\,\cos(\alpha\arg(\epsilon+i|\omega|))}{(\omega^2+\epsilon^2)\left(((\omega^2+\epsilon^2)^{\alpha}+1)(\omega^2+\epsilon^2)^{-\alpha/2}+2\cos(\alpha\arg(\epsilon+i|\omega|))\right)}. \tag{42}$$

Note that the term $\epsilon = Dq^2$ makes $\tilde{\phi}^{(\epsilon)}_{\mathrm{ML}}(\omega)$ regular at $\omega = 0$. In this context, it should be noted that the Lorentzian function that is weighted by the EISF in Eq. (41) tends to a Dirac distribution in the limit $\epsilon \to 0$.

IV. RESULTS AND DISCUSSION

The results shown in the following have been obtained by the fitting model (38) to the resolution-deconvoluted experimental intermediate scattering functions. To make the model parameters and functions explicitly appear, we write

$$F^{(+)}(q,t) = e^{-Dq^2 t}\left(EISF(q) + (1-EISF(q))E_\alpha\left(-(t/\tau)^\alpha\right)\right), \quad t \geq 0, \tag{43}$$

where

- D is the apparent translational diffusion coefficient,
- $EISF(q)$ determines the elastic intensity,
- $\alpha \equiv \alpha(q)$ sets the form of the relaxation function,
- $\tau \equiv \tau(q)$ sets the time scale of the relaxation function.

Fitting all four parameters at the same time is possible but leads to fits with large error bars, in particular, for the apparent translational diffusion coefficient, D. For this reason, we used the true translational diffusion coefficient obtained from dynamic light scattering (DLS) and, for comparison, the q-averaged diffusion coefficients, $\overline{D_{\mathrm{QENS}}(q)}$, from the four-parameter fit of the QENS spectra. Both fits give very similar values and confidence intervals for τ, α, and $EISF$, and we show here those for those with a fixed value for D_{DLS}. Table I shows both diffusion coefficients, where the error bars of $\overline{D_{\mathrm{QENS}}(q)}$ are given by the standard deviation of $D_{\mathrm{QENS}}(q)$ with respect to the mean value $\overline{D_{\mathrm{QENS}}(q)}$. The very small value of D_{DLS} for D_2O buffer at 323 K indicates the coagulation of MBP, and we

TABLE I. Diffusion coefficients from DLS and QENS for MBP in solvents I and II.

Temp (K)	$D_{\mathrm{DLS\,I}}$ (Å^2/ns)	$D_{\mathrm{QENS\,I}}$ (Å^2/ns)	$D_{\mathrm{DLS\,II}}$ (Å^2/ns)	$D_{\mathrm{QENS\,II}}$ (Å^2/ns)
283	3.31 ± 0.053	6.04 ± 0.46	2.05 ± 0.049	5.59 ± 0.73
293	5.72 ± 0.057	⋯	3.17 ± 0.145	⋯
303	7.49 ± 0.090	6.15 ± 0.80	4.42 ± 0.19	5.91 ± 0.70
313	9.85 ± 0.049	⋯	6,32 ± 0.292	⋯
323	0.31 ± 0.013	6.43 ± 0.83	8.15 ± 0.19	6.29 ± 0.36
	11.94 (extrapol.)			

show in the same position also the extrapolated value from lower temperatures for a non-coagulated solution.

The resulting three-parameter fits of the resolution-deconvoluted and symmetrized intermediate scattering function, $F^{(+)}(q,t)$, are shown in Fig. 2. All fits have been performed for the two solvents, D_2O buffer (solvent I) and D_2O buffer with 30% deuterated trifluoroethanol (TFE) (solvent II), and the three different temperatures, 283, 303, and 323 K. The blue data points

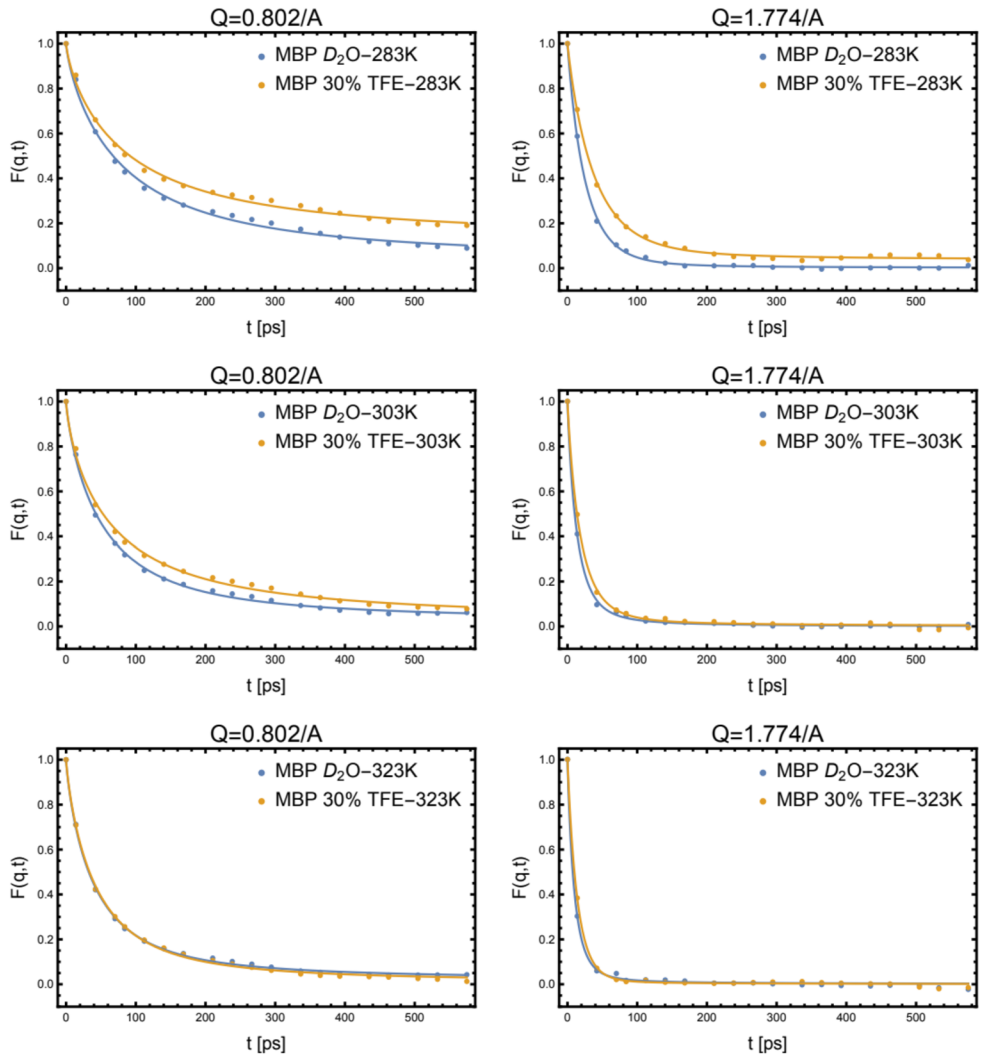

FIG. 2. Plot of the deconvoluted intermediate scattering function $F^{(+)}(q,t)$ of MBP at different temperatures, comparing solvents I and II (blue and dark yellow points, respectively), and the corresponding fits with model (43) (solid lines) for the minimum and maximum value of q.

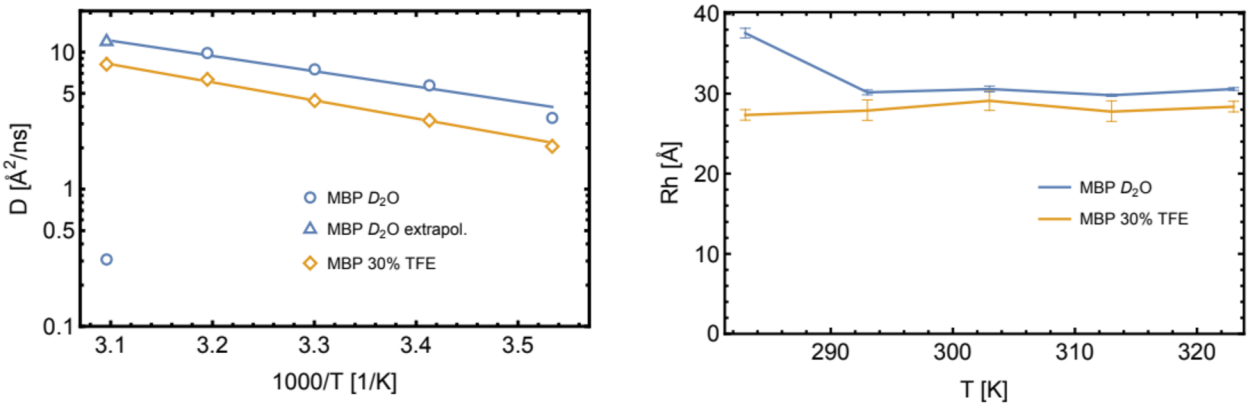

FIG. 3. Left panel: Arrhenius plot of the diffusion coefficient for MBP in solvent I (blue symbols) and solvent II (dark yellow symbols). The solid lines represent the corresponding fitted Arrhenius laws. Right panel: Effective hydrodynamic radii of MBP in the two solvents as a function of temperature.

correspond here to solvent I, the dark yellow points correspond to solvent II, and the corresponding solid lines label the fits. We note that not all data points have been used for the fits but a selection of points, which takes all data for $F(q,t)$ at short time lags and increasingly less points at large time lags. The reason is that the evaluation of the ML relaxation function is time consuming. We verified that that the resulting fit parameters are only weakly influenced by this choice.

We discuss first the results for the diffusion constants in the two buffers at the three temperatures, which have been obtained by DLS and QENS. We recall that MBP in D_2O buffer coagulates at 323 K, and we note in this context that the DLS experiments have been performed at lower protein concentrations than the QENS experiments (4 mg/ml for solvent I and 7 mg/ml for solvent II), which are thus certainly affected by coagulation. We are though confident that this phenomenon does not affect our results concerning the internal dynamics probed by the IN16B spectrometer since even setting $D = 0$, i.e., neglecting completely global diffusion in the fits of τ, α, and *EISF*, does only slightly alter the resulting values for τ, α, and *EISF*. The fits are though sensitive to deviating too much from the DLS and QENS values toward higher values. Replacing D_{DLS} for solvent I at 323 K by the extrapolated value from lower temperatures is not tolerated since the corresponding width Dq^2 for all q-values lies clearly outside the resolution of IN16B. The left panel of Fig. 3 shows an Arrhenius plot of the diffusion constants, where for solvent I at 323 K the extrapolated triangular data point has been used instead of the measured one. Here, the blue symbols refer again to solvent I and the dark yellow symbols refer to solvent II. The corresponding solid lines denote the fits of an Arrhenius law,[33,34]

$$D(T) = D_0 e^{-\frac{\Delta G}{k_B T}}, \tag{44}$$

where the activation energy is $\Delta G = 5.10$ kcal/mol for solvent I and $\Delta G = 6.05$ kcal/mol for solvent II. We note in this context that the activation energy for solvent I is close to the values that have been found for other IDPs[34] and corresponds to the activation energy for self-diffusion in liquid water.[35,36] The right panel of Fig. 3 shows an estimation of the effective hydrodynamical radius, R_h, of MBP as a function of temperature and solvent using the Stokes–Einstein relation

$$D = \frac{k_B T}{6\pi\eta R_h}, \tag{45}$$

with the diffusion coefficients from DLS and experimental values for the dynamic viscosity, η, which are given in the supplementary material. The viscosity was measured with a rolling ball viscometer for both solvents and the relevant temperature range (see the supplementary material). The results show that R_h is essentially constant with increasing temperature, and between 283 and 303 K, it

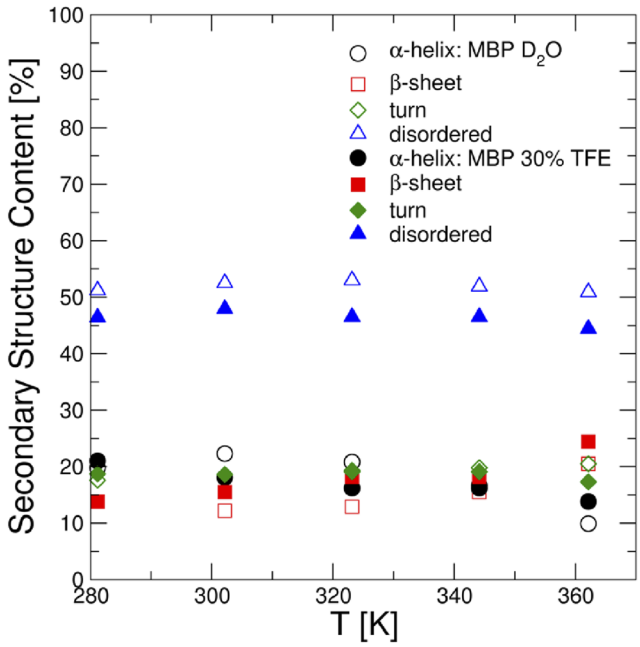

FIG. 4. Secondary structure content of MBP in solvent I (hollow symbols) and solvent II (full symbols).

decreases for MBP in D_2O buffer. Such a behavior has been, in fact, reported for IDPs,[37,38] but we will here not comment on that. The essential point is that no unfolding transition is observed with increasing temperature, which is characteristic for folded globular proteins. Figure 4 shows that this result is in agreement with the observation from CD spectroscopy that the secondary structure content is essentially constant over the whole temperature range, being slightly larger for the TFE-enriched buffer (solvent II). TFE is known to induce α-helical motives, and one can observe that at 283 K, but with increasing temperature, this effect disappears continuously, and at high temperatures it is even inverted. The effect of TFE consists thus in moving β-strands into α-helical motives and vice versa, keeping the total secondary structure content constant.

In Fig. 5, we show the fit parameters concerning the internal dynamics of MBP, comparing again the three different temperatures, 283, 303, and 323 K, and solvents I and II. The time scale parameter τ varies considerably with temperature and q, where the general rule is that it decreases with temperature and with q. This can be understood since lowering the temperature means slowing down the dynamics and since the higher values of q probe increasingly more localized and faster motions. The form parameter, α, of the relaxation function varies, in contrast, weakly with temperature and increases with q to values close to 1, indicating a close to exponential relaxation for localized motions. The particularly interesting result is that the relaxation dynamics of MBP in the two solvents becomes similar with increasing the temperature and is practically identical at 323 K. The observation is coherent with the observation that both the hydrodynamic radii and the content and composition of α-helices and β-strands are comparable. We also see that the coagulation of MBP, which is found by DLS in solvent I at 323 K and certainly present in the QENS samples of higher concentration, has no influence on the internal dynamics of the protein.

Concerning the EISF parameter, we observe that it is generally close to zero for the accessible q-range, except for solvent II at 283 K and small q-values, which indicates that at low temperatures solvent II hinders somewhat more large-amplitude motions compared to solvent I. We note in this context that EISFs are not systematically small for our model and refer to recent work on a QENS data

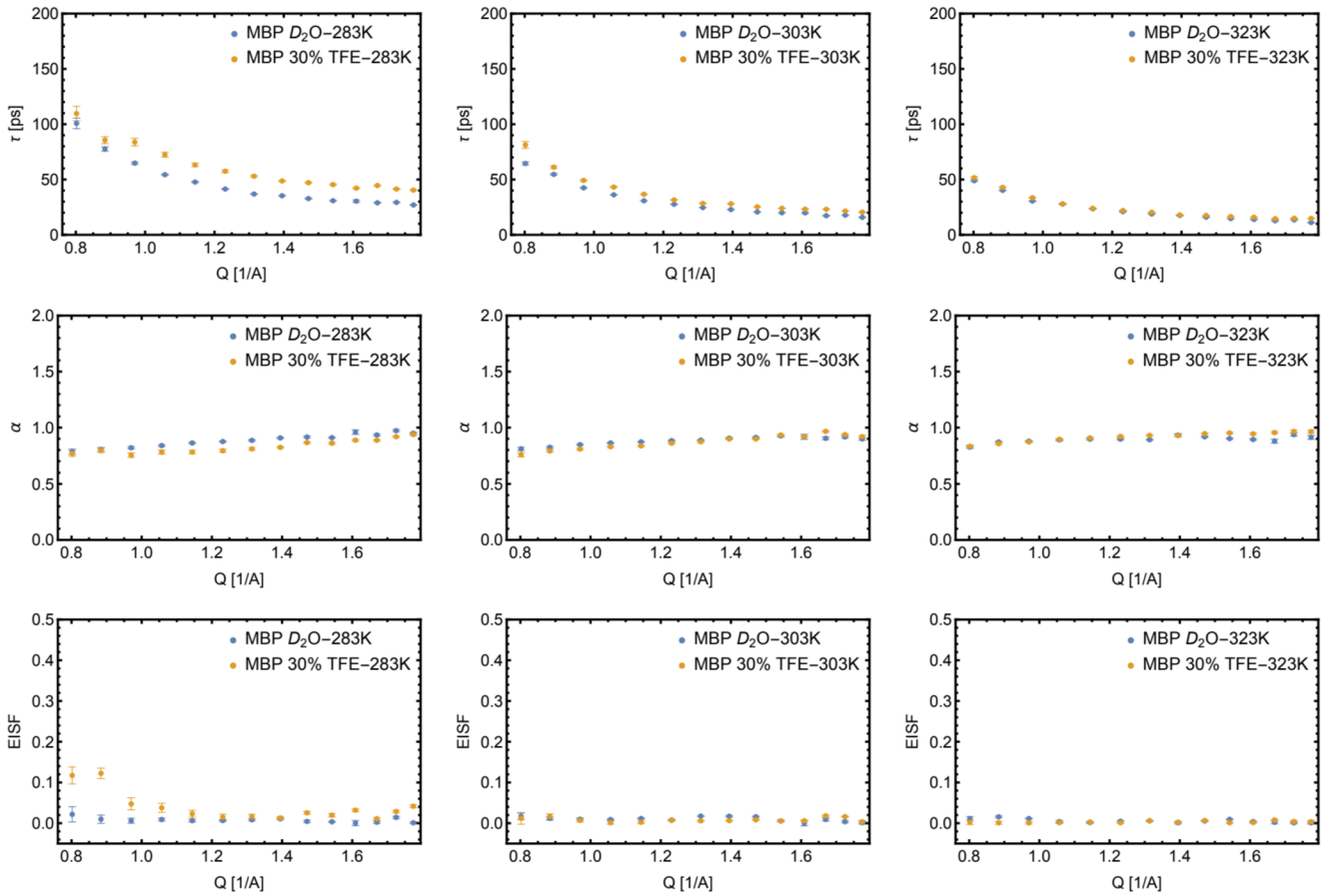

FIG. 5. From top to bottom, the model parameters τ, α, and *EISF* for MBP at different temperatures comparing the two solvents, D_2O buffer and D_2O buffer with 30% deuterated TFE.

analysis from hydrated powders of human acetylcholinesterase,[19,20] which is an enzyme with a well-defined structure. Here, the EISF was found to be clearly non-zero, as one would expect for such a protein that is more compact and such a sample, where global protein motions are prevented.

To complement the discussion of the fit parameters, we show in Fig. 6 the corresponding relaxation rate spectra, $p(\lambda)$, which are defined through Eq. (37). For both solvents and all temperatures, we observe that the peak of the relaxation rate spectrum shifts to higher values with increasing q, and its width decreases. This reflects the fact that the form parameter α approaches 1 with increasing q, noting that $\alpha = 1$ corresponds to exponential relaxation and a perfectly monodisperse relaxation rate spectrum of the form $p(\lambda) = \delta(\lambda - 1/\tau)$; we are now in the position to give a physical interpretation of the form parameter α, referring to the concept of protein energy landscapes proposed by Frauenfelder *et al.*[13] Proceeding as in Ref. 19, we consider the variable

$$\delta\xi(\mathbf{q},t) = \xi(\mathbf{q},t) - \langle\xi(\mathbf{q},t)\rangle, \quad \text{where} \quad \xi(\mathbf{q},t) = e^{i\mathbf{q}\cdot\mathbf{R}_j(t)}, \tag{46}$$

which is the spatial Fourier transform of the atomic density $\delta(\mathbf{r} - \mathbf{R}_j(t))$ of atom j, and assume that the dynamics of $\delta\xi(\mathbf{q},t)$ can be modeled as a fractional Ornstein–Uhlenbeck (fOU) process. The latter can be interpreted as the diffusion process in a "rough" parabolic potential, or "energy landscape," which tends to restore $\xi(\mathbf{q},t)$ to its mean value, $\langle\xi(\mathbf{q},t)\rangle$. Since $\xi(\mathbf{q},t)$ is a complex function, the real and the imaginary part should here be considered as independent variables, and the left panel of Fig. 7 depicts a sketch of the "rough" parabolic potential as a function of $\Re\{\delta\xi\}$ and $\Im\{\delta\xi\}$. If the variable $\delta\xi$ was diffusing in a smooth parabolic potential, then

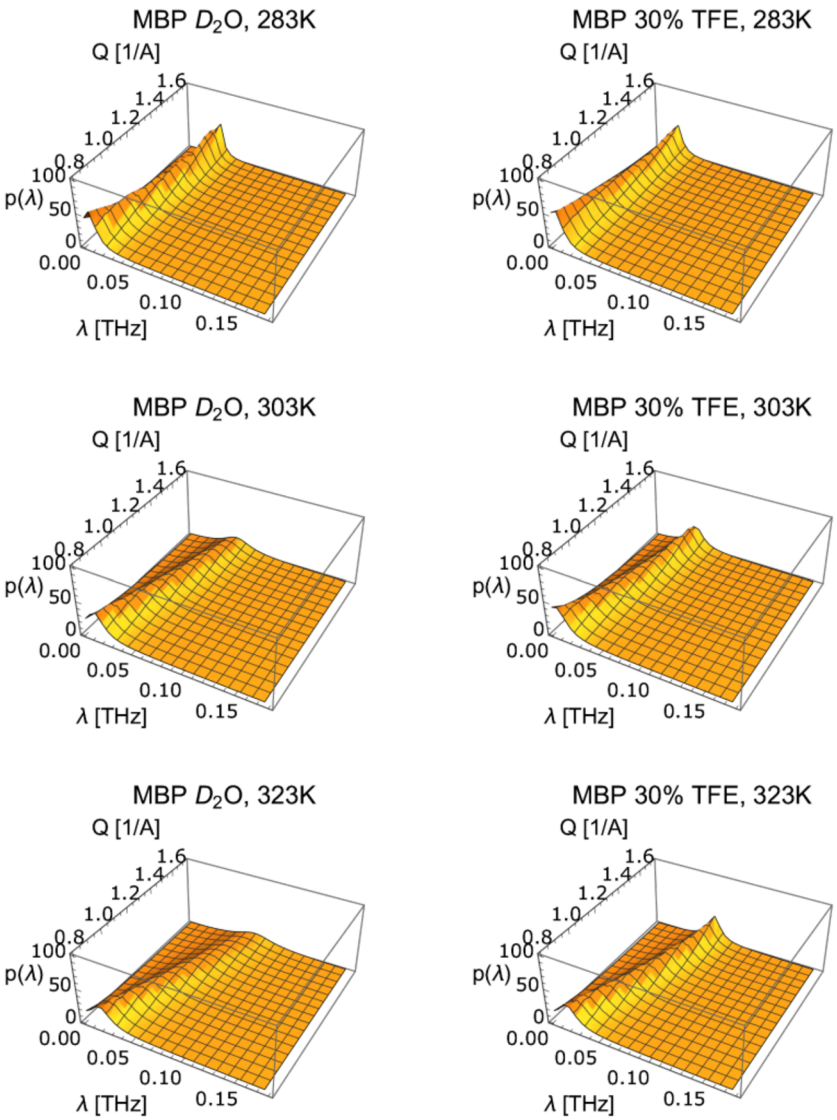

FIG. 6. From top to bottom, relaxation rate spectra $p(\lambda)$ [see Eq. (37)] for $T = 283$ K, $T = 303$ K, and $T = 323$ K, respectively, in D_2O buffer (left panel) and D_2O buffer with 30% TFE (right panel).

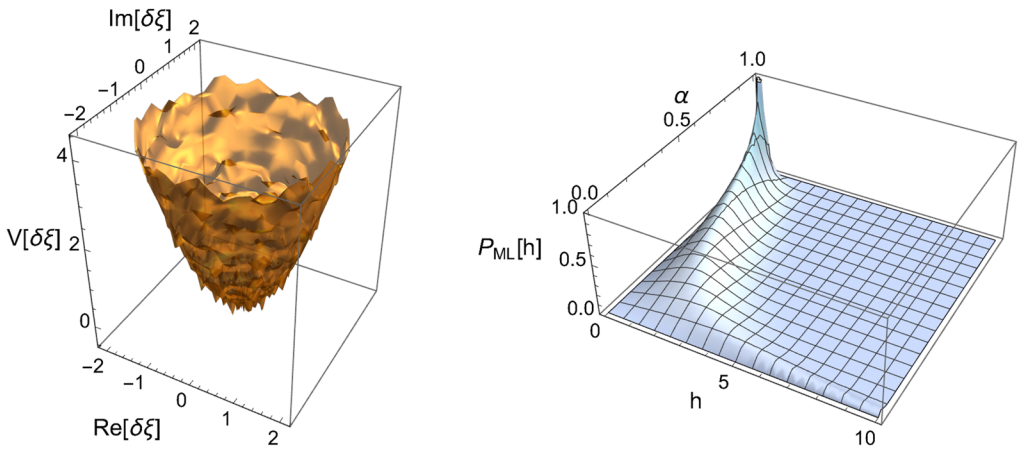

FIG. 7. Left panel: Sketch of a rugged harmonic potential for the real and imaginary part of $\delta\xi(\mathbf{q}, t)$. Right panel: Sketch of the energy barrier distribution, $P(h, \alpha)$, given in Eq. (48).

its time autocorrelation function would be an exponential function, $\langle \delta\xi^*(0)\delta\xi(t)\rangle \propto \exp(-t/\tau)$, and diffusion in the rugged potential leads to longtime memory effects, which are described by a ML relaxation function, i.e., $\langle \delta\xi^*(0)\delta\xi(t)\rangle \propto E_\alpha(-(t/\tau)^\alpha)$. As discussed in Ref. 19, one can find the distribution of the energy barriers in the "rough" parabolic potential by using the diffusion model proposed by Zwanzig,[39] which describes diffusion of a particle in a rough harmonic potential with a *fixed* energy barrier. Introducing the dimensionless energy barrier height

$$h = \frac{\Delta E}{k_B T}, \tag{47}$$

the distribution for the energy barriers corresponding to the ML relaxation function is found to be[19]

$$P_{\mathrm{ML}}(h) = \frac{2h\,\sin(\pi\alpha)}{\pi\left(e^{-\alpha h^2} + e^{\alpha h^2} + 2\,\cos(\pi\alpha)\right)}. \tag{48}$$

The right panel of Fig. 7 displays this distribution of energy barriers as a function of u and α. It shows that $\lim_{\alpha\to 1} P_{\mathrm{ML}}(h) = \delta(h)$, i.e., becomes more and more the energy barrier distribution for a smooth potential with vanishing barrier height, whereas for $\alpha \to 0$, the distribution $P_{\mathrm{ML}}(h)$ becomes very broad, including also barriers of almost infinite height. Having this interpretation in mind, the plots of the fit parameters shown in Fig. 5 show that localized motions are characterized by a smoother potential than global ones (α increases with q). This simply reflects that the relaxation rate spectrum of large-amplitude motions in a protein is more disperse than for localized motion since they require the concerted motion of many modes with different relaxation time scales. Concerning the influence of the solvent on the effective local potential of the hydrogen atoms, one sees that solvent II leads to a slightly rougher effective potential for $\delta\xi$ at T = 283 K compared to solvent I. This difference vanishes with increasing temperature, which makes the differences in the relaxation dynamics of MBP disappear.

V. CONCLUSIONS

The present analysis of high-resolution quasielastic neutron scattering spectra from myelin basic protein shows that "minimalistic" multiscale models for the relaxation dynamics of proteins combined with results from dynamic light scattering yield meaningful insights into the dynamics of intrinsically disordered proteins and permit, in particular, the detection and interpretation of changes in the relaxation dynamics as a function of solvent, temperature, and spatial resolution. With our choice of the Mittag-Leffler relaxation function as a model for the relaxation of the intermediate scattering function, the relaxation dynamics of MBP can be interpreted in terms of a simple energy landscape model. The QENS analysis shows that a trifluoroethanol-enriched solvent buffer at 283 K makes this energy landscape rougher, which leads to slower relaxation dynamics with a more disperse relaxation rate spectrum, and that this effect disappears continuously with increasing temperature. In accordance with this observation, the complementary experiments with dynamic light scattering and SRCD experiments show that TFE reduces at 283 K the radius of hydration of MBP and increases the α-helix content at the expense of β-strands. These effects disappear with increasing temperature, where the radii of hydration are comparable and constant, and at higher temperatures even more β-strands appear. Independent of if trifluoroethanol is added to the D_2O buffer or not, there is no unfolding transition with increasing temperature, which would manifest itself by a sudden increase in the hydrodynamic radius and which is typical for folded proteins. Our CD measurements confirm this observation, showing that the global secondary structure content in the presence of TFE is constant with temperature and only slightly higher compared to a pure D_2O buffer. To confirm our findings, small-angle x-ray scattering/small-angle neutron scattering (SAXS/SANS) will certainly be useful to obtain information about the radii of gyration and possible aggregation of MBP at exactly the same protein concentrations and solvents, which have been used for the QENS experiments.

From a technical point of view, we think that the high quality of the data and the extended energy transfer range of the IN16B

spectrometer with the new "BATS mode" (Backscattering And Time of flight Spectrometer) were crucial to obtain the results quoted above. We finally remark that all numerical and several analytical calculations have been performed with the Wolfram Mathematica package.[40]

SUPPLEMENTARY MATERIAL

In the supplementary material, we give information about complementary experiments by dynamic light scattering, viscosimetry, and synchrotron radiation circular dichroism spectroscopy on MBP as a function of solvent and temperature. We show, in particular, the global diffusion constants measured by DLS, the corresponding viscosities that have been used to compute the respective radii of hydration, and the SRCD spectra that have been used to evaluate the secondary structure content of MBP.

ACKNOWLEDGMENTS

We gratefully acknowledge beam time allocation for the neutron scattering experiments on the IN16B spectrometer at the Institut Laue-Langevin, Grenoble, France (http://doi.ill.fr/10.5291/ILL-DATA.8-04-874), and for the synchrotron radiation spectroscopy experiments on the DISCO beam line at the Synchrotron SOLEIL, Gif-sur-Yvette, France. In this context, we thank Frank Wien for his help with recording and analyzing the CD spectra.

A.N.H. acknowledges financial support from the Région Centre and the Jülich Center for Neutron Science.

AUTHOR DECLARATIONS

Conflict of Interest

The authors have no conflicts to disclose.

DATA AVAILABILITY

The neutron scattering data are available at http://doi.ill.fr/10.5291/ILL-DATA.8-04-874, and the SRCD data are available from the corresponding author upon reasonable request.

REFERENCES

[1] P. Tompa, Trends Biochem. Sci. **27**, 527 (2002).
[2] H. J. Dyson and P. E. Wright, Nat. Rev. Mol. Cell Biol. **6**, 197 (2005).
[3] P. Tompa, Trends Biochem. Sci. **37**, 509 (2012).
[4] P. E. Wright and H. J. Dyson, Nat. Rev. Mol. Cell Biol. **16**, 18 (2015).
[5] M. Vincenzi, F. A. Mercurio, and M. Leone, Curr. Protein Pept. Sci. **20**, 425 (2019).
[6] T. Springer, *Quasielastic Neutron Scattering for the Investigation of Diffusive Motions in Solids and Liquids* (Springer, Berlin, Heidelberg, 1972), Vol. 64, ISBN: 978-3-540-05808-3; 978-3-540-37457-2.
[7] M. Bée, *Quasielastic Neutron Scattering: Principles and Applications in Solid State Chemistry, Biology and Materials Science* (Adam Hilger, Bristol, 1988).
[8] J. Colmenero and A. Arbe, J. Polym. Sci., Part B: Polym. Phys. **51**, 87 (2013).
[9] A. M. Stadler, L. Stingaciu, A. Radulescu, O. Holderer, M. Monkenbusch, R. Biehl, and D. Richter, J. Am. Chem. Soc. **136**, 6987 (2014).
[10] L. R. Stingaciu, R. Biehl, D. Changwoo, D. Richter, and A. M. Stadler, J. Phys. Chem. Lett. **11**, 292 (2020).
[11] N. Alberding, R. H. Austin, S. S. Chan, L. Eisenstein, H. Frauenfelder, I. C. Gunsalus, and T. M. Nordlund, J. Chem. Phys. **65**, 4701 (1976).
[12] R. H. Austin, K. W. Beeson, L. Eisenstein, H. Frauenfelder, and I. C. Gunsalus, Biochemistry **14**, 5355 (1975).
[13] W. Doster, S. Cusack, and W. Petry, Nature **337**, 754 (1989).
[14] I. E. T. Iben, D. Braunstein, W. Doster, H. Frauenfelder, M. K. Hong, J. B. Johnson, S. Luck, P. Ormos, A. Schulte, P. J. Steinbach *et al.*, Phys. Rev. Lett. **62**, 1916 (1989).
[15] H. Frauenfelder, S. G. Sligar, and P. G. Wolynes, Science **254**, 1598 (1991).
[16] W. G. Glöckle and T. F. Nonnenmacher, Biophys. J. **68**, 46 (1995).
[17] H. Yang and X. S. Xie, J. Chem. Phys. **117**, 10965 (2002).
[18] H. Yang, G. Luo, P. Karnchanaphanurach, T.-M. Louie, I. Rech, S. Cova, L. Xun, and X. S. Xie, Science **302**, 262 (2003).
[19] S. C. Kou and X. S. Xie, Phys. Rev. Lett. **93**, 180603 (2004).
[20] G. R. Kneller, Proc. Natl. Acad. Sci. U. S. A. **115**, 9450 (2018).
[21] M. Saouessi, J. Peters, and G. R. Kneller, J. Chem. Phys. **150**, 161104 (2019).
[22] M. Saouessi, J. Peters, and G. R. Kneller, J. Chem. Phys. **151**, 125103 (2019).
[23] E. H. Eylar and M. Thompson, Arch. Biochem. Biophys. **129**, 468 (1969).
[24] M. Appel, B. Frick, and A. Magerl, Sci. Rep. **8**, 13580 (2018).
[25] M. Appel, B. Frick, and A. Magerl, Physica B **562**, 6 (2019).
[26] O. Arnold, J. C. Bilheux, J. M. Borreguero, A. Buts, S. I. Campbell, L. Chapon, M. Doucet, N. Draper, R. Ferraz Leal, M. A. Gigg *et al.*, Nucl. Instrum. Methods Phys. Res., Sect. A **764**, 156 (2014).
[27] S. Lovesey, *Theory of Neutron Scattering from Condensed Matter* (Clarendon Press, Oxford, 1984), Vol. I.
[28] A. M. Stadler, F. Demmel, J. Ollivier, and T. Seydel, Phys. Chem. Chem. Phys. **18**, 21527 (2016).
[29] P. Schofield, Phys. Rev. Lett. **4**, 239 (1960).
[30] *Mittag-Leffler Functions, Related Topics and Applications*, *Springer Monographs in Mathematics*, edited by R. Gorenflo, A. A. Kilbas, F. Mainardi, and S. V. Rogosin (Springer, Heidelberg, 2014), ISBN: 978-3-662-43929-6; 978-3-662-43930-2.
[31] G. R. Kneller, Phys. Chem. Chem. Phys. **7**, 2641 (2005).
[32] V. Calandrini, V. Hamon, K. Hinsen, P. Calligari, M.-C. Bellissent-Funel, and G. R. Kneller, Chem. Phys. **345**, 289 (2008).
[33] K. Sozański, A. Wiśniewska, T. Kalwarczyk, and R. Hołyst, Phys. Rev. Lett. **111**, 228301 (2013).
[34] I. V. Nesmelova, D. L. Melnikova, V. Ranjan, and V. D. Skirda, *Progress in Molecular Biology and Translational Science* (Elsevier, 2019), Vol. 166, pp. 85–108, ISBN: 978-0-12-816851-6.
[35] D. W. McCall, D. C. Douglass, and E. W. Anderson, J. Chem. Phys. **31**, 1555 (1959).
[36] R. Mills, J. Phys. Chem. **77**, 685 (1973).
[37] M. Kjaergaard, A.-B. Nørholm, R. Hendus-Altenburger, S. F. Pedersen, F. M. Poulsen, and B. B. Kragelund, Protein Sci. **19**, 1555 (2010).
[38] R. Wuttke, H. Hofmann, D. Nettels, M. B. Borgia, J. Mittal, R. B. Best, and B. Schuler, Proc. Natl. Acad. Sci. U. S. A. **111**, 5213 (2014).
[39] R. Zwanzig, Proc. Natl. Acad. Sci. U. S. A. **85**, 2029 (1988).
[40] Wolfram Research, Inc., Mathematica, Version 12.0, Champaign, IL, 2019.